View metadata, citation and similar papers at core.ac.uk
brought to you by CORE
provided by NASA Technical Reports Server

Comparison of the impact of the Arctic Oscillation and East Atlantic/West Russia teleconnection on interannual variation in East Asian winter temperatures and monsoon

Young-Kwon Lim[1] and Hae-Dong Kim[2]

[1] NASA Goddard Space Flight Center, Goddard Earth Sciences Technology and Research (GESTAR)/ I. M. Systems Group, Greenbelt, Maryland, U.S.A.
(Email: Young-Kwon.Lim@nasa.gov)

[2] College of Environment, Keimyung University, Daegu, South Korea
(Email: khd@kmu.ac.kr)

Corresponding author: Hae-Dong Kim

July 10, 2014
Submitted to Theoretical and Applied Climatology

Abstract

The large-scale impacts of the Arctic Oscillation (AO) and the East Atlantic/West Russia (EA/WR) teleconnection on the East Asian winter climate anomalies are compared for the past 34 winters focusing on 1) interannual monthly to seasonal temperature variability, 2) East Asian winter monsoon (EAWM), and 3) the Siberian high (SH) and cold surge. Regression analysis reveals warming by AO and EA/WR over mid-latitude East Asia during their positive phase and *vice versa*. The EA/WR impact is found to be comparable to the AO impact in affecting the East Asian temperature and monsoon. For example, warm (cold) months over mid-latitude East Asia during the positive (negative) AO are clearly seen when the AO and EA/WR are in the same phase. Near zero correlation is found between temperature and the AO phase when both teleconnections are in an opposite phase. The well-known negative relationship between SH and the AO phase is observed significantly more often when the AO is in the same phase with the EA/WR. Also, the indices of EAWM, cold surge, and SH are found to be more highly negative-correlated with the EA/WR rather than with the AO. The advective temperature change and associated circulation demonstrate that the anomalous large-scale field including the SH over the mid-latitude Asian inland is better represented by the EA/WR, influencing the East Asian winter climates. These results suggest that the impact of EA/WR should be considered more important than previously thought for a better understanding of East Asian winter temperature and monsoon variability.

1. Introduction

The impact of planetary-scale circulation patterns (i.e., teleconnection) on East Asian winter temperature variability have been explored in many studies, focusing primarily on the Arctic Oscillation (AO) (Jeong and Ho 2005; Park et al. 2011) or El Niño Southern Oscillation (ENSO) (Chen et al. 2004). However, recent studies argue a decreasing role of ENSO (He et al. 2013) and an increasing role of other large-scale patterns originating in the Northern Hemispheric mid-latitudes or the Arctic for influencing East Asian winter temperatures. For example, Lim et al. (2012) and Liu et al. (2012) found the importance of the Arctic sea ice variation to drive an anomalously warm or cold winter over East Asian region. Another important factor that possibly affects East Asian winter temperature is the teleconnection patterns originating in the North Atlantic. Several studies have suggested the impact of these teleconnections on East Asian winter climate variability via large-scale Rossby wave propagation (Bueh and Nakamura 2009; Wang et al. 2011; Kim et al. 2014). The East Atlantic/West Russia (EA/WR) (Barnston and Livezey 1987; Washington et al. 2000) teleconnection is a good example, characterized by a well-organized Rossby wave propagation pattern spanning the European continent, Siberia, and East Asia. However, the importance of EA/WR in determining East Asian winter temperatures has not attracted any significant or detailed investigations. Few studies have critically examined the dynamic mechanism responsible or assessed the significance of the impact, compared with the relatively well-understood dominant impact, such as that of the AO.

The AO (Thompson and Wallace 1998) is understood to be a dominant teleconnection, affecting East Asian winter monsoon (EAWM) variability (Gong et al. 2001; Li and Yang 2010). However, Wang et al. (2011) suggested the possible role of EA/WR in modulating

EAWM variability. That study found a correlated structure between meridional wind anomalies over East Asia in the winter and sea surface temperatures in the preceding summer over the North Atlantic, which the study presumed was the source region for the EA/WR-like teleconnection pattern. We also suggest that a large-scale pressure anomaly in central Russia, driven by the EA/WR, can affect the EAWM significantly (Kim et al. 2014). This pressure pattern is strongly related to the Siberian high, and as noted by Wu and Wang (2002b) and Chen et al. (2014), this Siberian pressure anomaly may not be significantly correlated with the AO for influencing the EAWM. These arguments in earlier studies suggest that it is important to compare the impact of EA/WR and AO on the variability of East Asian winter temperature and monsoon.

The present study was motivated by the present limited understanding of the role of EA/WR in modulating East Asian winter temperatures and monsoon variability. In this study, we intend to quantitatively estimate the impact of EA/WR and AO through various analysis methods (e.g., the rotated empirical orthogonal function (REOF) technique (Richman 1986), regression, correlation, and composite analysis). The degree of these teleconnections' contributions to East Asian winter temperature is then compared by investigating atmospheric anomalies (e.g., height, circulation, and advective temperature change process) for the four different phase composites, AO(+)EA/WR(+), AO(+)EA/WR(-), AO(-)EA/WR(+), and AO(-)EA/WR(-), to better identify their relative importance in modulating East Asian winter temperature and EAWM variability.

Section 2 describes the dataset and analysis method used. Estimation of the impact of AO and EA/WR on temperature variability is addressed in Section 3. Section 3 also compares the impact of EA/WR and AO on EAWM activity and the related cold surge, followed by a summary and discussion in Section 4.

2. Data and methods

The primary analytical methods used in this study are the REOF technique (Richman 1986), correlation, regression, and composite analysis. The REOF was applied to upper-tropospheric monthly height data archived at the Modern Era Retrospective analysis for Research and Applications (MERRA) reanalysis (Rienecker et al. 2011). The analysis time period covers the past 34 winters from December-February (DJF) 1979/80 through DJF 2012/13. The horizontal resolution of the data is 0.5° (latitude) × 0.6667° (longitude). Lower-level (850 hPa) wind and temperature data were used to investigate the thermal advective process over the East Asian domain. We also used 2-m level MERRA temperature data to compare temperature anomalies induced by the impact of AO and EA/WR, respectively, with the observed temperature anomalies. Several indices were used, including the East Asian winter monsoon index (EAWMI) (Jhun and Lee 2004; Li and Yang 2010), the cold surge index (CSI) (Chang et al. 2005), and the Siberian high index (SHI) (Panagiotopoulos et al. 2005) to investigate the impact of EA/WR and AO on interannual variation of EAWM and the cold surge.

3. Results

a. Impact of AO and EA/WR on East Asian winter temperature

Large-scale teleconnection patterns of AO and EA/WR were captured using the upper level (250 hPa) geopotential height for the domain that spans Eurasia. The monthly climatological cycle of the height field for DJF was removed and the REOF technique was applied to capture the leading teleconnection patterns. The data were area-weighted as a function of cosine latitude before applying the REOF technique. The reason for selecting the 250 hPa pressure level is that the large-scale mass distribution linked to the polar jet stream is typically located near the 250-300 hPa level in the winter.

The AO and EA/WR teleconnection patterns were identified for large domain that covers North Atlantic and Eurasia (100°W-160°E, 10°S-90°N), explaining ~22% (AO: ~12%, EA/WR: ~10%) of the total monthly 250 hPa height variance, respectively. Anomalies were plotted on a positive phase basis in Figures 1a and 1d. The sum of their percentage variance tended to be sensitive to a slight domain change, but it varied within the range of 20-25%. Also, we repeated the modal separation by including the entire Northern Hemisphere (NH) to clarify the robustness of the spatial patterns shown in Figures 1a and 1d. The captured AO and EA/WR patterns from the entire NH domain are superimposed by contours in Figures 1a and 1d, confirming the robustness of the patterns with the domain change. We compare the principal component (PC) time series with the corresponding teleconnection time series, available from the National Center for Environmental Prediction (NCEP)/Climate Prediction Center (CPC) (ftp://ftp.cpc.ncep.noaa.gov/wd52dg/data/indices/tele_index.nh) to further confirm that the teleconnection patterns captured here are reliable. Figures 1b and 1e clearly demonstrate realistic capture of AO and EA/WR teleconnections, yielding a high temporal correlation, exceeding 0.6. Calculation for the seasonally averaged PC time series and teleconnection indices produced correlations near 0.7 (data not shown for seasonal mean PC time series).

The spatial distribution of the AO consists of the zonally symmetric alternating anomalies in the Arctic and the Northern Hemispheric mid-latitudes (Fig. 1a) (Thompson and Wallace 1998). It is clear that an easterly anomaly crossing the southern part of Japan and Korea is feasible during the positive phase, whereas the negative phase favors a westerly anomaly along mid-latitude East Asia (30-40°N) that could transport a continental cold air mass to this region.

The EA/WR pattern in Figure 1d consists of two large-scale anomalies over Europe, located in Western Europe and Russia, north of the Caspian Sea (Barnston and Livezey 1987; Washington et al. 2000; Wang et al. 2011), and an anomaly over the mid-latitude Asian sector. The pattern appears to have a large-scale wave propagation structure, spanning the Atlantic, Europe, western Russia, and East Asia. The positive height anomaly over East Asia north of 40°N, with the negative anomaly south of it, implies an anticyclonic circulation with the easterly anomaly from the Pacific along 35-40°N during the positive phase, whereas the opposite is true for the negative phase.

Actual temperature anomalies associated with AO and EA/WR are quantitatively estimated, respectively, by regressing the monthly 2-m air temperature anomalies onto the monthly teleconnection PC time series. Regressed temperature anomalies for the AO mode $A_{AO}(x, y)$, for example, were calculated based on the following equation.

$$A_{AO}(x, y) = \sum_{t=1}^{tot} T(x, y, t) \cdot P_{AO}(t)$$

Here $T(x, y, t)$ is the temperature anomaly field at grid point (*x*,*y*) and time *t*, and $P_{AO}(t)$ is the normalized monthly PC time series of the z250 height for the AO mode. *tot* in the above summation is equal to 102 months, the length of the analysis period. Figure 1c demonstrates that the AO impact spans the most of Eurasia region. The strongest temperature response is found over central Siberia (~90°E and ~60°N), showing temperature increase (decrease) more than 2K by a strong southerly (northerly) wind in the event of the positive (negative) AO phase. Temperature anomalies over the East Asia region are found primarily in all areas north of 40°N and some areas south of 40°N (e.g., Korea, Japan, and the Shandong peninsula in China), with the magnitude of temperature anomalies greater than 1K north of 45°N. This AO impact tends to be relatively weak over the southern part of East Asia, such as the area south of Shandong (~35°N).

Figure 1f shows a positive temperature response to the positive EA/WR, spanning Northern China, Mongolia, Russia, near Lake Baikal, Korea and Japan, whereas a cold temperature response is true for the negative EA/WR. Specifically, the impact of EA/WR tends to be strong in Russia, near Lake Baikal, with a temperature magnitude greater than 1K. With the magnitude smaller than 1K, the areas affected by EA/WR with statistical significance over East Asian mid-latitudes are Korea, Japan, and northern China, north of 35°N.

The impact of AO and EA/WR was compared to identify their relative importance for determining East Asian winter temperature variability. We reconstructed the two sets of monthly temperature data, one of which contains only the AO impact and the other contains the EA/WR impact only. Data reconstruction was completed by a linear combination of the regressed temperature anomalies and corresponding teleconnection time series. For example, the reconstructed field $R_{AO}(x,y,t)$ for the AO mode at grid point (x,y) and time t is defined as

$$R_{AO}(x,y,t) = A_{AO}(x,y) \cdot P_{AO}(t),$$

where $A_{AO}(x,y)$ is the regressed temperature anomaly field for AO mode and

$P_{AO}(t)$ represents the normalized monthly PC time series of the z250 hPa height for the AO mode. We then calculated the spatial correlation between the reconstructed temperatures and observed temperature anomalies in each year for the East Asian domain, covering primarily eastern China, Korea, and Japan (110-150°E, 20-60°N). Figure 2 is a time series of the resulting spatial correlation values over all 34 winters. The red line, representing the correlation of temperatures due to AO impact with the observations, reveals reasonable reproduction of the observed East Asian winter temperature variability, producing a correlation average of 0.38 over all 34 winters. The blue line, representing the EA/WR impact, has a correlation of 0.36. More critical inspection of these time series through partial correlation that separately considers the first 15 years and the most recent 15 years reveals significant correlation difference between the two periods for the EA/WR. The averaged correlation with the EA/WR for the first 15 years covering 1980s and early 1990s is just 0.3. The correlation value increases to 0.45 for the period of the most recent 15 years that covers the late 1990s and the early 21st century, indicating an increased dependence of East Asian temperature on the EA/WR phase in recent years. In contrast, the partial correlation with the AO is nearly unchanged (corr.= 0.35-0.40) over different periods (e.g., earlier 15 years vs. later 15 years).

Figures 2b through 2g show the anomalous winter temperature distribution for two selected recent years for example. Figures 2b through 2d show the result for the 2007-08 winter, when the AO impact was dominant in determining the East Asian winter temperature, while the impact of EA/WR was very small due to a near-neutral phase. Figures 2e through 2g show the winter temperature distributions for the 2011-12 winter, when the EA/WR impact was more decisive in determining the East Asian winter temperature anomaly. It is clear that the temperature anomalies distribution by EA/WR impact (Fig. 2f) is quite close to the observed temperature distribution (Fig. 2g). Although anomalous temperature distribution for another recent winters of 2009-10 and 2012-13 is not shown in this paper, Figure 2a indicates that temperatures in those two winters were substantially explained by both AO (Wen et al. 2013) and EA/WR with spatial correlation near 0.8.

b. Linear relationship of teleconnection with EAWM, Siberian high, and cold surge

East Asian winter temperatures are influenced largely by the frequency and intensity of cold surges, which are closely linked to the EAWM. Previous studies have argued a dominant role for AO in determining the EAWM activity and cold surges (Gong et al. 2001; Wang et al. 2005; Park et al. 2011). Park et al. (2011) also addressed, however, that occurrence of cold surges, in the form of a wave train was little related to the AO phase, indicating that we still need clarification as to whether the AO phase is a predominant factor in determining EAWM activity and cold surges over East Asia.

In this section, we compare the impact of AO with the impact of EA/WR on 1) EAWM, 2) the cold surge, and 3) the Siberian high to assess whether the impact of AO is really the dominant factor in determining variation in the three features. We first defined the EAWM index (EAWMI) (Fig. 3, red-solid line) following Jhun and Lee (2004) and Li and Yang (2010), based on variations in the upper-level westerly jet over East Asia. We found that those two indices are highly correlated (r = 0.87). Table 1 shows temporal correlations between teleconnection indices (EA/WR and AO) and EAWMI time series. Negative correlation values indicate a strong EAWM during the negative phase of EA/WR and AO, and *vice versa*. It is clear that EAWMI has a stronger negative correlation with the EA/WR (-0.59) than with the AO (-0.24). Stronger negative correlations with the EA/WR are also found for the cold surge index (CSI; Fig. 3, red-dashed line) and the Siberian high index (SHI; Fig. 3, red-dotted line), discussed in more detail later. Figure 3 shows that all indices (EAWMI, CSI, SHI, -EA/WR, and -AO) exhibit upward trends for the periods ~1988/89 to 2012/13 winter. Calculating the correlation after removing this linear upward trend over the ~25 winters once again produced a stronger negative correlation with the EA/WR (~ -0.35) than with the AO (~ -0.10), which is no longer significant. This low correlation with the AO is consistent with Jhun and Lee (2004) and Wu et al. (2006) who suggested little correlation between AO and EAWM on an interannual time scale.

Atmospheric spatial patterns regressed onto the EAWMI were calculated and then compared with those regressed onto the negative phase of EA/WR and AO, respectively. Figure 4 clearly shows that strong EAWM over East Asia is characterized by below-average temperature (Fig. 4a), northerly flow coming from Siberia and the northwestern Pacific (Fig. 4b), enhanced upper-level westerly in mid-latitudes (~20°-40°N; Fig. 4c) and upper-level continental convergence and oceanic divergence (Fig. 4d). The spatial distributions of these patterns are quite close to the regressed patterns associated with the negative EA/WR, shown in Figures 5a-c. The temperature distribution in Figure 4a also significantly resembles the pattern in Figure 1f multiplied by -1, indicating a strong EAWM during the negative EA/WR and *vice versa*. Figures 5d-f represent the negative AO impact and exhibit similar spatial distributions to those associated with EAWMI (Fig. 4), but the similarity between them is relatively weaker than that between the negative EA/WR (Figs. 5a-c) and EAWMI (Fig. 4). For example, the magnitude of upper level westerly anomalies and their locations, shown in Figure 4c, are better explained by Figure 5b than by Figure 5e. The pressure distribution with the sea-land contrast and large-scale anomaly centered over Siberia seen in Figure 4b is better reproduced by Figure 5a than by Figure 5d. Upper-level divergent/convergent flow between the Asian continent and the northwestern Pacific, which is a typical characteristic of large-scale monsoon circulation, is also better structured in Figure 5c than in Figure 5f. These characteristic differences imply a connection between EAWM and EA/WR comparable to, or closer than, the connection between EAWM and AO. Spatial correlations (90°-150°E and 20°-60°N) in Table 2 clarify that EAWM activity has a closer connection with the phase of EA/WR than with the AO. These results differ somewhat from several studies that have argued a dominant role for AO in determining the EAWM intensity (e.g., Gong et al. 2001; Wu and Wang 2002a). However, Gong et al. (2001) also suggested a significant contribution of the Eurasian teleconnection pattern (e.g., EA/WR) to better explain the interannual variation of EAWM and the Siberian high.

EAWM activity is also understood to be an indicator of cold surge activity (Jhun and Lee 2004; Li and Yang 2010). Chang et al. (2005) defined CSI for the South China Sea and southeastern Asia using the meridional wind component. We applied that definition to the mid-latitudes for the domain of 90°-130°E and 40°-60°N, which covers northeastern Asia and the eastern side of the Siberian high. The CSI was defined as the area-averaged meridional wind over this spatial domain (Fig. 3, red-dashed line). This region was selected because it is a good pathway for the meridional wind coming from the Northern high-latitudes towards mid-latitude East Asia. Note that meridional wind components were multiplied by -1 so that the CSI value is positive during the cold surge year and *vice versa*. Regressed patterns associated with the CSI were found to resemble Figure 4, demonstrating that the EAWM is an indicator of cold surge activity over East Asia (Fig. 6). The temporal correlation between CSI and EAWMI is 0.77. Table 3 clearly demonstrates a stronger relationship between the cold surge and negative EA/WR than with the negative AO, which is in good agreement with the conclusion in Table 2.

The reason for the higher correlation between the EAWMI and CSI with the EA/WR than with the AO seems to be associated with a better representation of the Siberian high pressure variation due to the impact of EA/WR than AO. This, in turn, indicates that the Siberian high may not be closely linked to AO only (Wu and Wang 2002b). For confirmation, we calculated the Siberian high index (SHI), following Panagiotopoulos et al. (2005) and Hasanean et al. (2013), and then examined its correlation with the EA/WR and AO, respectively.

The temporal correlation between SHI versus CSI and SHI versus EAWMI is 0.81 and 0.69, respectively, over the last 34 winters, indicating that the Siberian high is strongly coupled with the winter monsoon and cold winters over East Asia (Gong and Ho 2002). The spatial distributions regressed onto SHI shown in Figure 7 are nearly consistent with the patterns regressed onto EAWMI (Fig. 4). Spatial correlations (90°-150°E and 20°-60°N) between SHI and two teleconnections (EA/WR and AO) shown in Table 4 demonstrate that EA/WR better represents the variation in the Siberian high than does AO. Cheung et al. (2012) described the dominant role of Ural-Siberian blocking in influencing the EAWM. The pressure pattern associated with the blocking (Fig. 3a in Cheung et al. (2012)) resembled the typical pattern of EA/WR over Russia.

c. Atmospheric features for the four different combinations of AO and EA/WR phases

Monthly temperature anomaly area-averaged over East Asia is scatter-plotted with respect to the AO phase in Figure 8. We selected the months when both AO and EA/WR indices exceeded 0.5 in magnitude out of the entire 102 (34 years × 3 months) months. In total, 31 and 18 months were found, respectively, for cases where the AO and EA/WR are in the same phase (blue dots in Fig. 8) and in the opposite phase (red dots). Scatter plots indicate that a positive relationship between the temperature anomaly and AO phase is found clearly when the AO and EA/WR are in the same phase (blue dots). The correlation between the temperature anomaly and the AO phase is 0.48. The correlation drops markedly, to 0.09, when the two teleconnections are in the opposite phase. This indicates that East Asian winter temperature anomalies are *not* determined simply by the AO phase alone. This scatter plot also supports Figure 2, in arguing that the interannual temperature variation over East Asia is to a great extent influenced by the phase of EA/WR as well as AO.

Figure 9 is the same as Figure 8 but for the investigation of the Siberian high activity with respect to the AO phase. Figure 9 clearly demonstrates that well-known negative relationship between the Siberian high and AO phase (Wang et al. 2005) is pronounced only when the EA/WR is in the same phase as the AO (Corr. = -0.45). This negative correlation with the Siberian high is significantly reversed to the positive correlation (Corr. = 0.24) when the AO phase is opposite to the EA/WR phase. Because this correlation value is obtained by correlating positive (negative) Siberian high anomaly to the negative (positive) EA/WR phase, this positive correlation indicates stronger dependency of the Siberian high activity on the EA/WR phase rather than on the AO phase in our analysis period.

Atmospheric circulation and advective temperature change are examined in Figures 10 and 11 to further demonstrate our argument. Upper-level geopotential height and wind fields are plotted in Figure 10 for the four different composites, AO(+)EA/WR(+), AO(+)EA/WR(-), AO(-)EA/WR(+), and AO(-)EA/WR(-). When both AO and EA/WR are in the positive phase, a positive height anomaly in conjunction with the anomalous southeasterly flow from the Pacific is dominant over East Asia, implying warm conditions (Fig. 10a). This atmospheric pattern is nearly reversed when both the AO and EA/WR are in the negative phase, causing a cold surge due to strong wind flow from the high-latitude Asian continent (Fig. 10d). When the two teleconnections are in the opposite phase, warm atmospheric condition in the positive AO and *vice versa* is no longer obvious over the mid-latitude East Asia, as seen in Figures 10c for the positive AO and 10b for the negative AO. Interestingly, atmospheric circulation anomalies over the Asian inland (e.g., Russia (Siberia)) tend to be determined more by the EA/WR phase, as the strong cyclonic circulation with the negative height anomaly is observed in Figures 10a and 10b (positive EA/WR), while the anticyclonic circulation with the positive height anomaly is observed in Figures 10c and 10d (negative EA/WR). In contrast to the Asian continent, the atmospheric height anomaly in the Arctic sea is strongly determined by the AO phase.

The same characteristic feature, that the EA/WR tends to dominantly represent the Asian inland atmospheric patterns, is also found from the advective temperature change at lower levels (850 hPa). Figure 11 represents the circulation and regressed lower-level (850 hPa) temperature advection [K day^{-1}] by anomalous winds. It is evident that temperature advection is better represented by the EA/WR phase than the AO phase, as Figures 11a and 11b (positive EA/WR) show the positive advection whereas the negative advection over the Asian inland is seen in Figures 11c and 11d (negative EA/WR). The mid-latitude East Asian region is also characterized by warm advection in the positive EA/WR phase and cold advection in the negative EA/WR phase. Particularly, a closer association of the pattern of temperature advection with the EA/WR phase, versus the AO phase, in Figures 11b and 11c, suggests that the EA/WR impact could sometimes overwhelm the impact of AO. This argument appears consistent with the conclusions of several earlier studies that the impact of AO alone does not fully explain the variation in the Siberian high (Wu and Wang 2002b) and the EAWM activity on an interannual time scale (Jhun and Lee 2004).

4. Summary and Discussion

In this study, we compared the impacts of AO- and EA/WR-related climate anomalies (monthly to seasonal time scale) on the variability of East Asian winter temperature and monsoon over the past 34 years. Statistically significant temperature anomalies, which are associated with one standard deviation in each teleconnection time series, based on linear regression, were found with a 0.5-1K amplitude over mid-latitude East Asia. It was clearly found through regression analysis that the positive AO and EA/WR have warming effects on mid-latitude East Asian winter temperatures, whereas the negative phase has a cooling effect. The EAWM, Siberian high, and cold surge tend to be negatively correlated with the phases of AO and EA/WR.

The present study suggests that the conventional understanding that AO is the most dominant teleconnection to affect EAWM may need to be reconsidered. A series of comparisons between the impact of EA/WR and AO on EAWM activity, the cold surge, and the Siberian high in this study reveal that the EA/WR impact is comparable to or could sometimes be stronger than the AO impact for resolving interannual variation of East Asian winter climates. The EA/WR modulates the variation in the Siberian high more effectively than the AO does. As evidenced by correlations, regression, and composite patterns in this study, variations in the Siberian high and corresponding monsoon circulation, which leads to a warmer/colder winter over East Asia, is more accurately reproduced by the EA/WR impact, although the AO impact also explains them reasonably. Composite patterns with respect to the phases of AO and EA/WR also demonstrate that EA/WR is more influential than AO over the Asian inland (e.g., Ural mountains area and Siberia) for characterizing the anomalous monthly temperature, Siberian high, large-scale atmospheric circulation and temperature advection, which affect the winter climate over mid-latitude East Asia.

One might argue a probable inter-relationship between AO and EA/WR, although we capture them as independent modes with simultaneous relation considered. The correlation between AO and EA/WR seasonal mean indices obtained from NCEP/CPC is 0.30 for our 34 year analysis period, which lies near the limit of statistical significance at the 5% level. It appears not easy to argue strongly, based on this correlation, that the teleconnections could interact with each other. The source region of the EA/WR pattern is known to be the Atlantic Ocean (Barnston and Livezey 1987) and it is not clearly understood yet whether this activity over the Atlantic Ocean has any relationship with the AO. Wang et al. (2011) suggested a relationship between the EA/WR and El Niño, rather than AO, by showing that the EA/WR-related winter circulation over East Asia affected circulation over the western Pacific in the following season, which can help initiate a Pacific El Niño. The possibility of a relationship between these two teleconnections will need clarification in future studies.

In conclusion, the evidence presented here suggests that the impact of EA/WR needs to be considered more important than previously thought for a better understanding of the interannual variations in East Asian winter temperature, monsoon, and associated cold surges. Investigation of the EA/WR should further be complemented by more detailed studies, including the prediction of EA/WR teleconnection. Diabatic heating (or cooling) processes over the Atlantic and/or the Atlantic storm track activity, which are known to be the key factors for generating the EA/WR pattern (Franzke and Feldstein 2005; Lim 2014), still need to be thoroughly understood for more realistic predictions of the East Asian winter temperatures and monsoon.

Acknowledgement

This research was supported by the Scholar Research Grant of Keimyung University in 2013.

References

Barnston AG, Livezey RE (1987) Classification, seasonality and persistence of low-frequency atmospheric circulation patterns. Mon Wea Rev 115: 1083-1126

Bueh C, Nakamura H (2007) Scandinavian pattern and its climate impact. Quart J Royal Meteor Sci 133: 2117-2131

Chang CP, Harr PA, Chen HJ (2005) Synoptic disturbances over the equatorial South China Sea and western maritime continent during boreal winter. Mon Wea Rev 133: 489-503

Chen TC, Huang WR, Yoon JH (2004) Interannual variation of the East Asian cold surge activity. J Climate 17: 401-413

Chen Z, Wu R, Chen W (2014) Distinguishing interannual variations of the northern and southern modes of the East Asian winter monsoon. J Climate 27: 835-851

Cheung HM, Zhou W, Mok HY, Wu MC (2012) Relationship between Ural-Siberian blocking and the East Asian winter monsoon in relation to the Arctic oscillation and the El Niño-Southern oscillation. J Climate 25: 4242-4257

Franzke C, Feldstein SB (2005) The continuum and dynamics of Northern Hemispheric teleconnection patterns. J Atmos Sci 62: 3250-3267

Gong DY, Wang SW, Zhu JH (2001) East Asian winter monsoon and Arctic Oscillation. Geophys Res Lett 28: 2073-2076

Gong DY, Ho CH (2002) Siberian high and climate change over middle to high latitude Asia. Theor App Climatol 72: 1-9

Hasanean HM, Almazroui M, Jones PD, Alamoudi AA (2013) Siberian high variability and its teleconnectios with tropical circulations and surface air temperature over Saudi Arabia. Clim Dyn 41: 2003-2018 doi:10.1007/s00382-012-1657-9

He S, Wang H, Liu J (2013) Changes in the relationship between ENSO and Asia-Pacific midlatitude winter atmospheric circulation. J Climate 26: 3377-3393

Jeong JH, Ho CH (2005) Changes in occurrence of cold surges over East Asia in association with Arctic Oscillation. Geophys Res Lett 32 L14704 doi:10.1029/2005GL023024

Jhun JG, Lee EJ (2004) A new East Asian winter monsoon index and associated characteristics of the winter monsoon. J Climate 17: 711-726

Kim Y, Kim KY, Park S (2014) Seasonal scale variability of the East Asian winter monsoon and the development of a two-dimensional monsoon index. Clim Dyn 42: 2159-2172 doi:10.1007/s00382-013-1724-x

Li Y, Yang S (2010) A dynamical index for the East Asian winter monsoon. J Climate 23: 4255-4262

Lim YK, Ham YG, Jeong JH, Kug JS (2012) Improvement in simulation of Eurasian winter climate variability with realistic Arctic sea ice condition in an atmospheric GCM. Env Res Lett 7: 044041(6pp) doi:10.1088/1748-9326/7/4/044041

Lim YK (2014) The East Atlantic West Russia teleconnection in the North Atlantic: Climate impact and relation to Rossby wave propagation. Clim Dyn (in review)

Liu J, Curry JA, Wang H, Song M, Horton RM (2012) Impact of declining Arctic sea ice on winter snowfall. PNAS 109: 4074-4079

Panagiotopoulos F, Shahgedanova M, Hannachi A, Stephenson D (2005) Observed trends and teleconnections of the Siberian High. J Climate 18: 1411-1422

Park TW, Ho CH, Yang S (2011) Relationship between the Arctic Oscillation and cold surges over East Asia. J Climate 24: 68-83

Richman MB (1986) Rotation of principal components. J Climatol 6: 293–335

Rienecker MM, Coauthors (2011) MERRA – NASA's Modern-Era Retrospective Analysis for Research Applications. J Climate 24: 3624-3648

Thompson DWJ, Wallace JM (1998) The Arctic oscillation signature in the wintertime geopotential height and temperature fields. Geophys Res Lett 25(9): 1297-1300 doi:10.1029/98GL00950

Wang D, Wang C, Yang X, Lu J (2005) Winter Northern Hemisphere surface air temperature variability associated with the Arctic Oscillation and North Atlantic Oscillation. Geophys Res Lett 32: L16706 doi:10.1029/2005GL022952

Wang X, Wang C, Zhou W, Wang D, Song J (2011) Teleconnected influence of North Atlantic sea surface temperature on the El Niño onset. Clim Dyn 37: 663-676 doi:10.1007/s00382-010-0833-z

Washington R, Hodson A, Isaksson E, Macdonald O (2000) Northern hemisphere teleconnection indices and the mass balance of Svalbard glaciers. Int J Climatol 20: 473-487

Wen XY, Hu YY, Liu JP (2013) The extremely colde 2009-2010 winter and its relationship with the Arctic oscillation. Fron Phys 8: 590-603

Wu B, Wang J (2002a) Possible impacts of winter Arctic Oscillation on Siberian high, the East Asian winter monsoon and sea-ice extent. Advan Atmos Sci 19: 297-320

Wu B, Wang J (2002b) Winter Arctic Oscillation, Siberian high and East Asian winter monsoon. Geophys Res Lett 29 doi:10.1029/2002GL015373

Wu B, Zhang R, D'Arrigo R (2006) Distinct modes of the East Asian winter monsoon. Mon Wea Rev 134: 2165-2179

Table 1. Temporal correlations of the East Asian winter monsoon index (EAWMI), cold surge index (CSI), and Siberian high index (SHI) with teleconnection indices (EA/WR and AO).

	EA/WR	**AO**
EAWMI	**-0.59**	**-0.24**
CSI	**-0.54**	**-0.27**
SHI	**-0.57**	**-0.21**

Table 2.
Second row: Spatial correlations between the regressed atmospheric patterns onto the EAWMI and EA/WR. Third row: Same as the second row but for the regressed patterns onto the EAWMI and AO. Regressed patterns are calculated for five atmospheric variables, respectively, as they are listed in the first row of the table.

	T2m	**UV850**	**SLP**	**U300**	**Velp**
EAWMI vs. EA/WR	**-0.87**	**-0.86**	**-0.97**	**-0.92**	**-0.86**
EAWMI vs. AO	**-0.66**	**-0.62**	**-0.56**	**-0.59**	**-0.72**

Table 3

Second row: Spatial correlations between the regressed atmospheric patterns onto the CSI and EA/WR. Third row: Same as the second row but for the regressed patterns onto the CSI and AO. Regressed patterns are calculated for five atmospheric variables, as they are listed in the first row of the table.

	T2m	UV850	SLP	U300	Velp
CSI vs. EA/WR	**-0.85**	**-0.84**	**-0.95**	**-0.92**	**-0.91**
CSI vs. AO	**-0.60**	**-0.57**	**-0.54**	**-0.60**	**-0.68**

Table 4

Second row: Spatial correlations between the regressed atmospheric patterns onto the SHI and EA/WR. Third row: Same as the second row but for the regressed patterns onto the SHI and AO. Regressed patterns are calculated for five atmospheric variables, as they are listed in the first row of the table.

	T2m	UV850	SLP	U300	Velp
SHI vs. EA/WR	**-0.92**	**-0.69**	**-0.97**	**-0.95**	**-0.71**
SHI vs. AO	**-0.74**	**-0.62**	**-0.53**	**-0.65**	**-0.65**

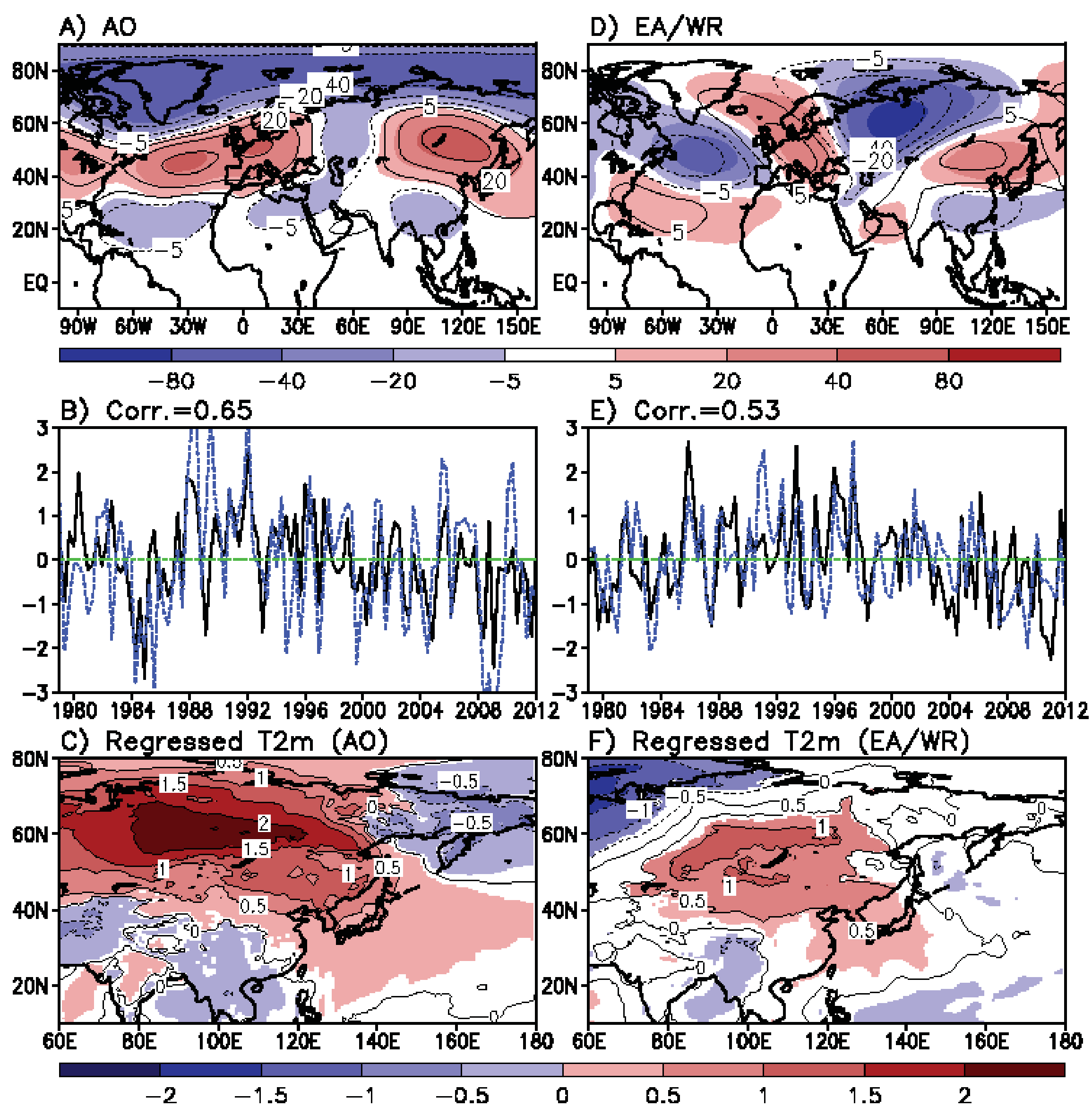

Figure 1. Top panel: Shading represents the non-normalized rotated empirical orthogonal functions (REOFs) of the monthly 250 hPa height [m] archived from a MERRA reanalysis. The analysis period included the last 34 winters from December to February (DJF) 1979/80 through DJF 2012/13. Superimposed contours are the REOFs extracted for the entire Northern hemispheric domain. Middle panel: The corresponding PC time series (solid lines). Dashed lines indicate the teleconnection indices time series of AO (left) and EA/WR right), respectively, archived at NOAA/NCEP/CPC. Bottom panel: Distribution of the regressed 2-m air temperature anomalies [K] onto each teleconnection. Temperatures statistically significant at the 10% level are shaded.

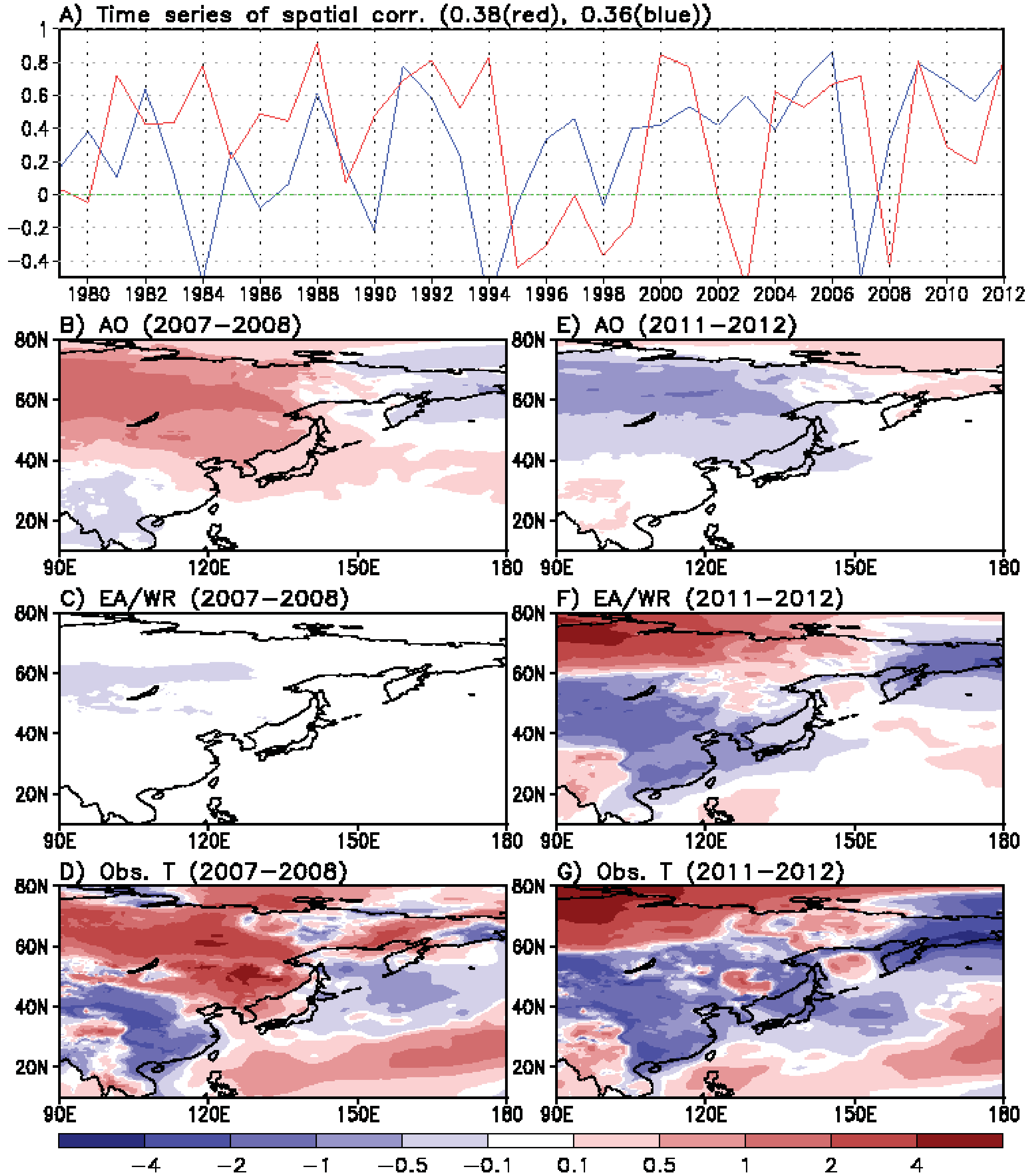

Figure 2. Upper: Time series of the spatial correlation coefficients between observed temperature anomalies (temporal anomalies) and the reconstructed temperatures consisting of AO impact (red) and EA/WR impact (blue), respectively, for the mid-latitudes East Asian domain (110°-150°E, 20°-60°N). B) and E) represent the winter temperature anomalies by the impact of AO for 2007-08 (B) and 2011-12 (E). (C) and (F) are the same as (B) and (E) but for the anomalies caused by the impact of EA/WRA. Observed temperature anomaly distributions for those years are shown in (D) and (G) for comparison.

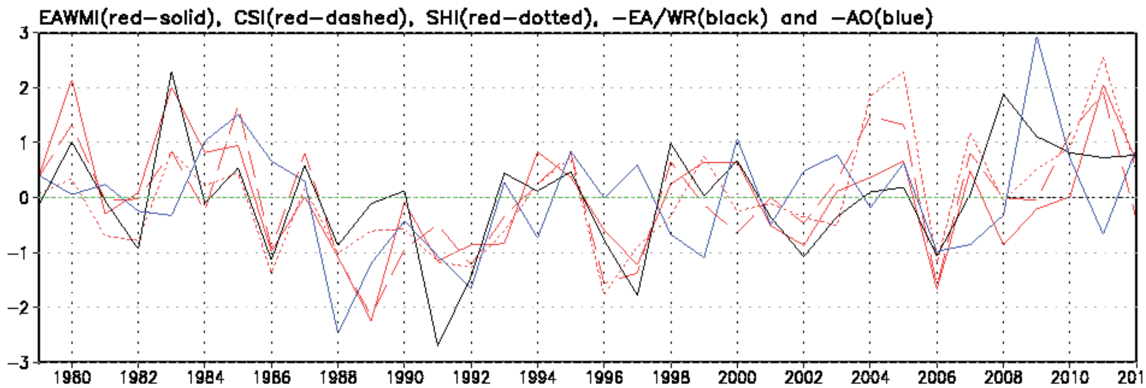

Figure 3. Interannual variation in normalized EAWMI, CSI, SHI, -EA/WR, and -AO. They are denoted by red-solid, red-dashed, red-dotted, black solid, and blue solid lines, respectively.

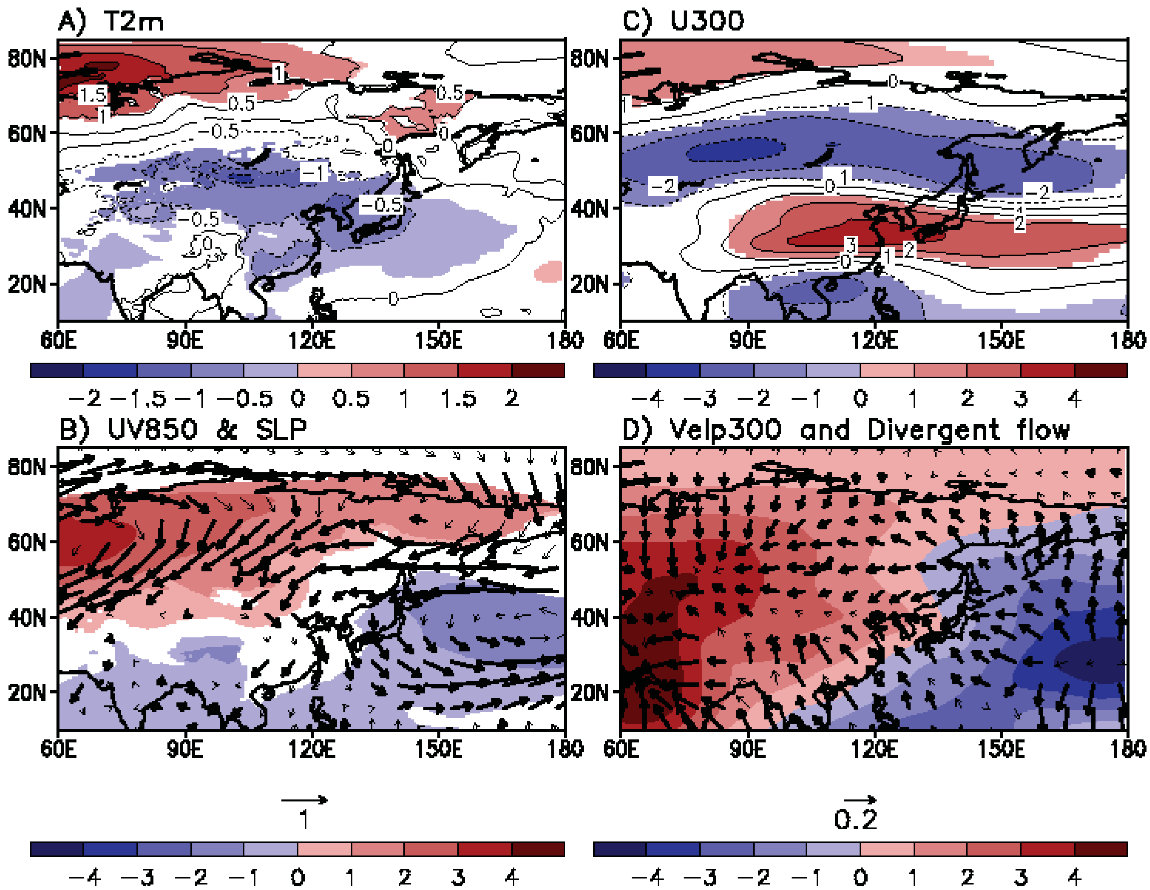

Figure 4. Horizontal distributions of atmospheric variables regressed onto EAWMI. Except velocity potential [1.0e+5 m^{2}s^{-1}] on the lower-right panel, the shaded area indicates where the values are significant at the 10% level. Thick arrows on the bottom panel (B and D) indicate vectors significant at the 10% level.

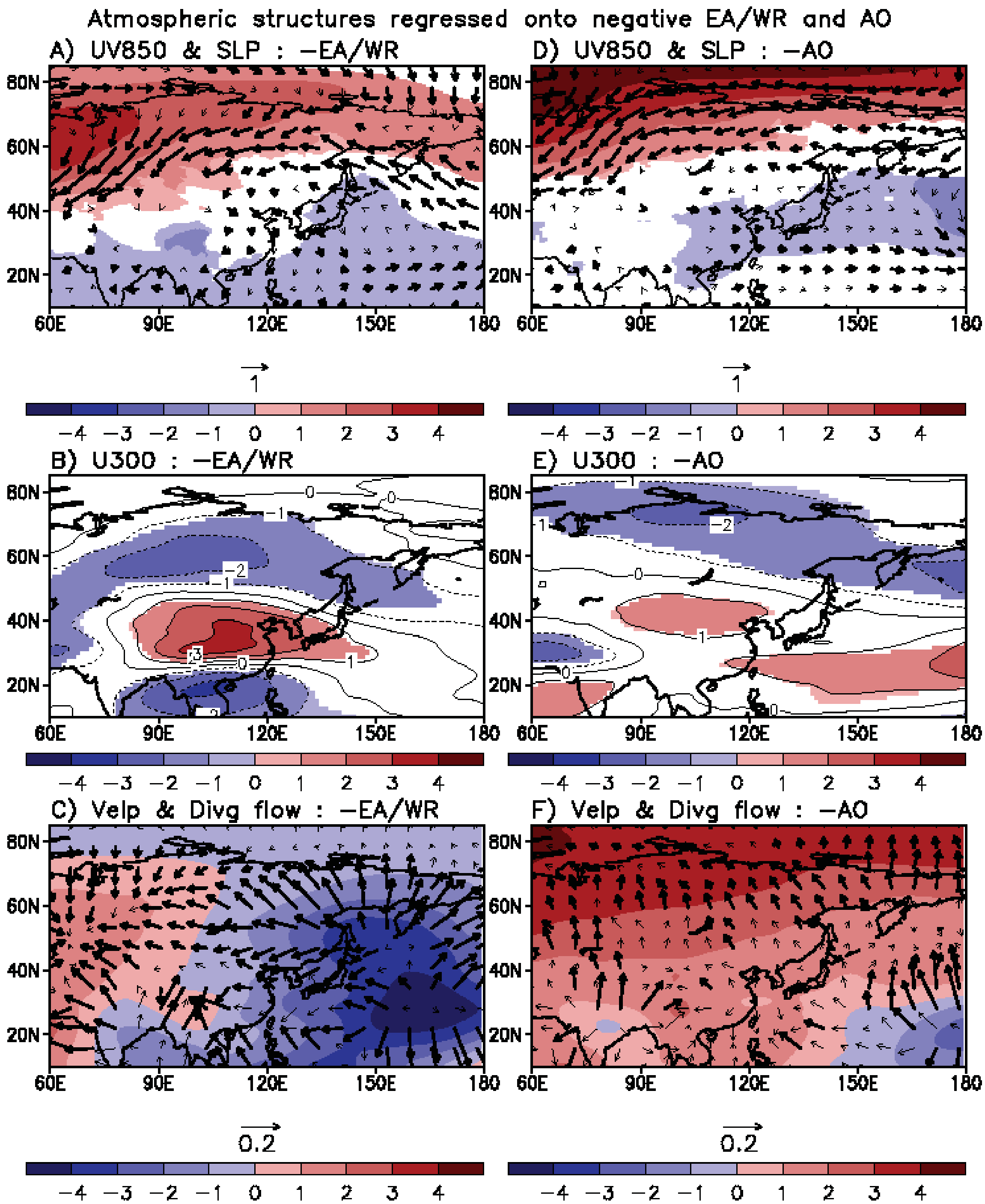

Figure 5. Horizontal distributions of atmospheric variables regressed onto -EA/WR (left) and -AO (right). Except velocity potential [1.0e+5 m^2s^{-1}] on the bottom panel (C and F), shaded area indicates where values are significant at the 10% level. Thick arrows on the top (A and D) and bottom panel (C and F) indicate vectors significant at the 10% level.

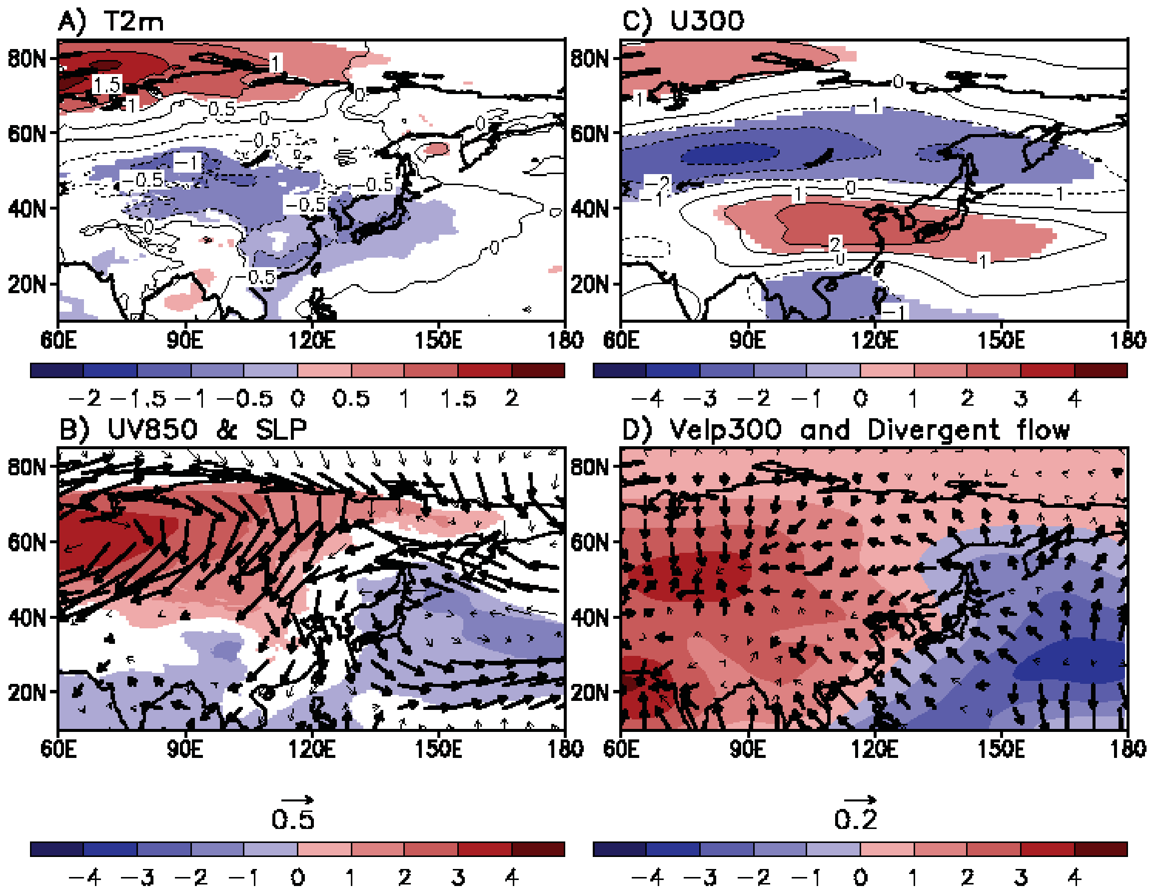

Figure 6. Same as Figure 4 but for regression onto CSI.

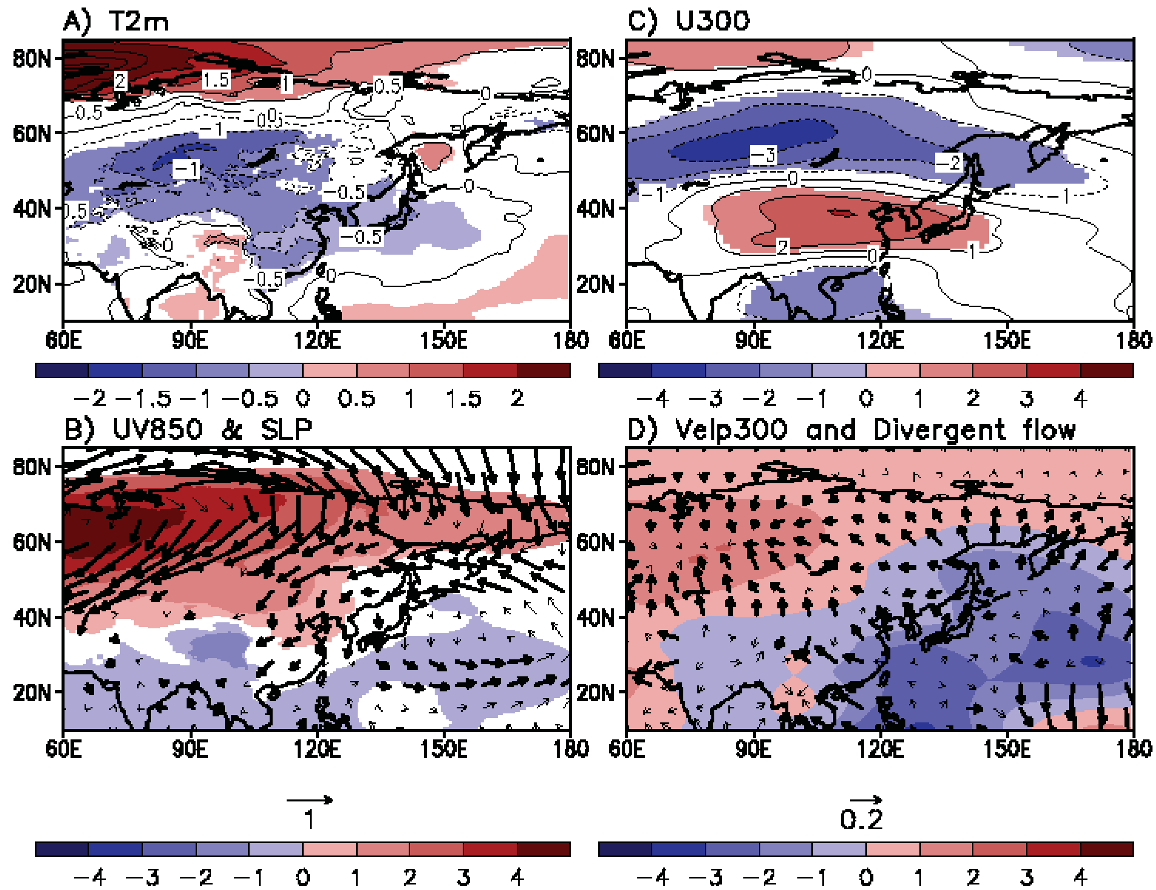

Figure 7. Same as Figure 4 but for regression onto SHI.

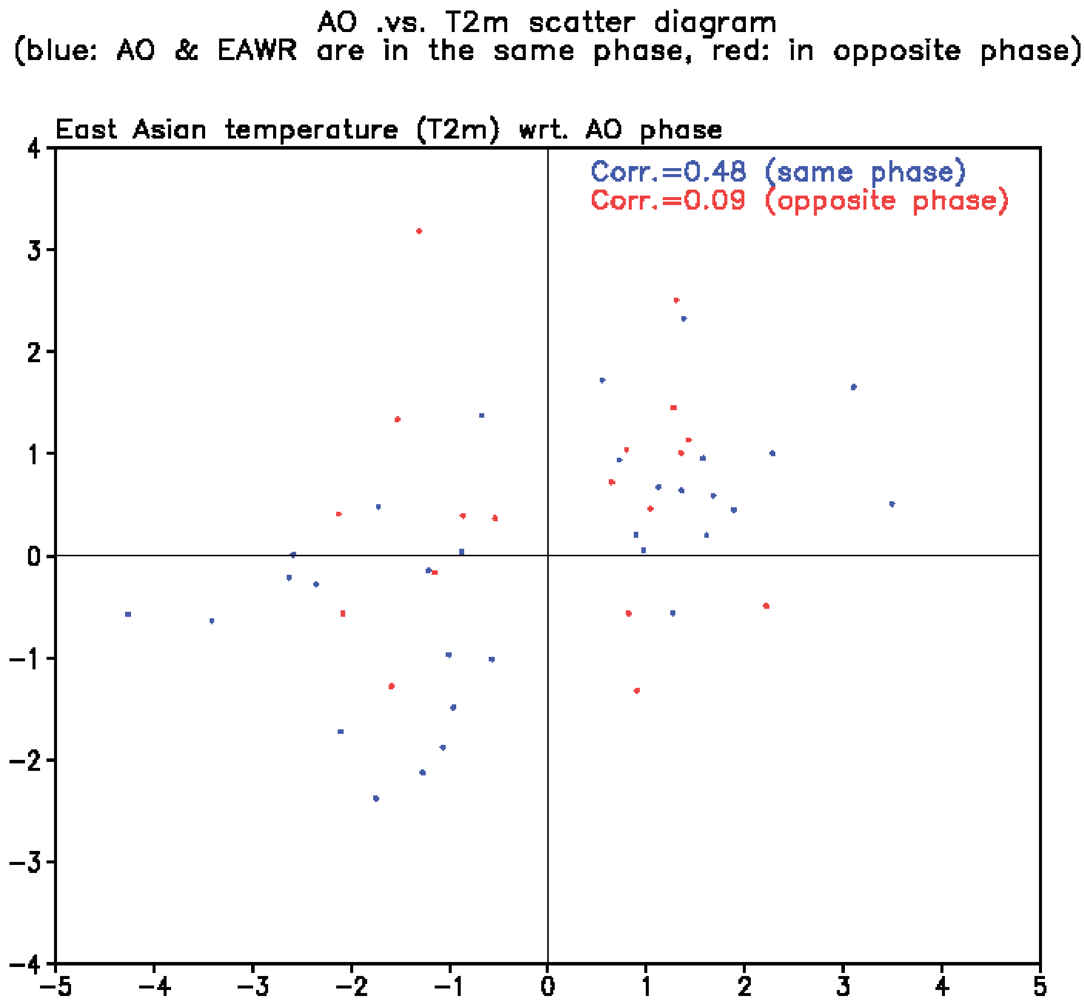

Figure 8. Scatter plots between the 2-m air monthly temperature anomaly area-averaged over the mid-latitude East Asia (100°-150°E, 30V-50°N) and AO phase. The temperature anomalies for the months when both AO and EA/WR are in the same phase are plotted in blue, while the anomalies for the months when AO and EA/WR are in the opposite phase are plotted in red. Note that the months when the magnitude of AO and EA/WR indices were both greater than 0.5 were used in the scatter plot.

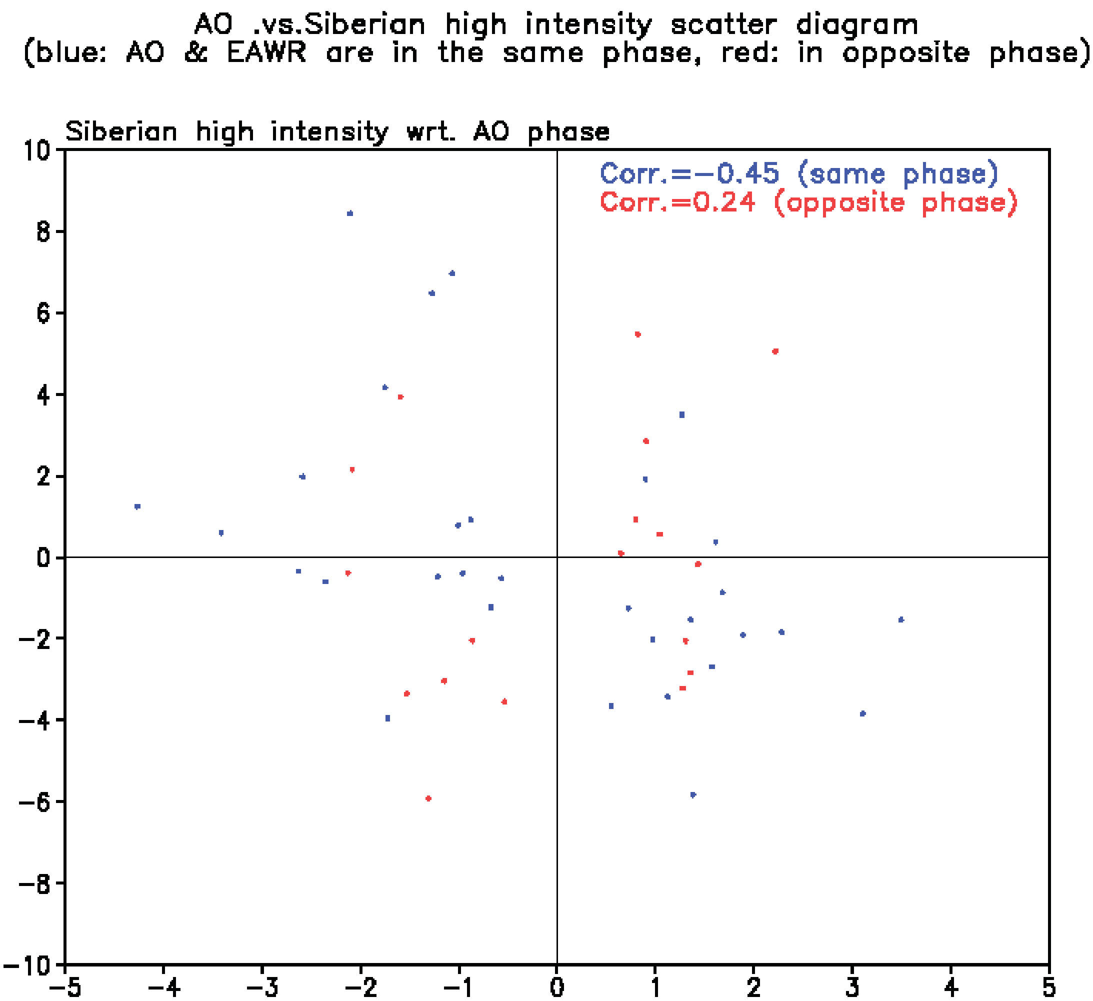

Figure 9. Same as Figure 8 but for switching 2-m air temperature anomaly to the Sea level pressure anomaly area-averaged over the domain of 80°-120°E and 20°-45°N, which is the same as the domain for the Siberian high index.

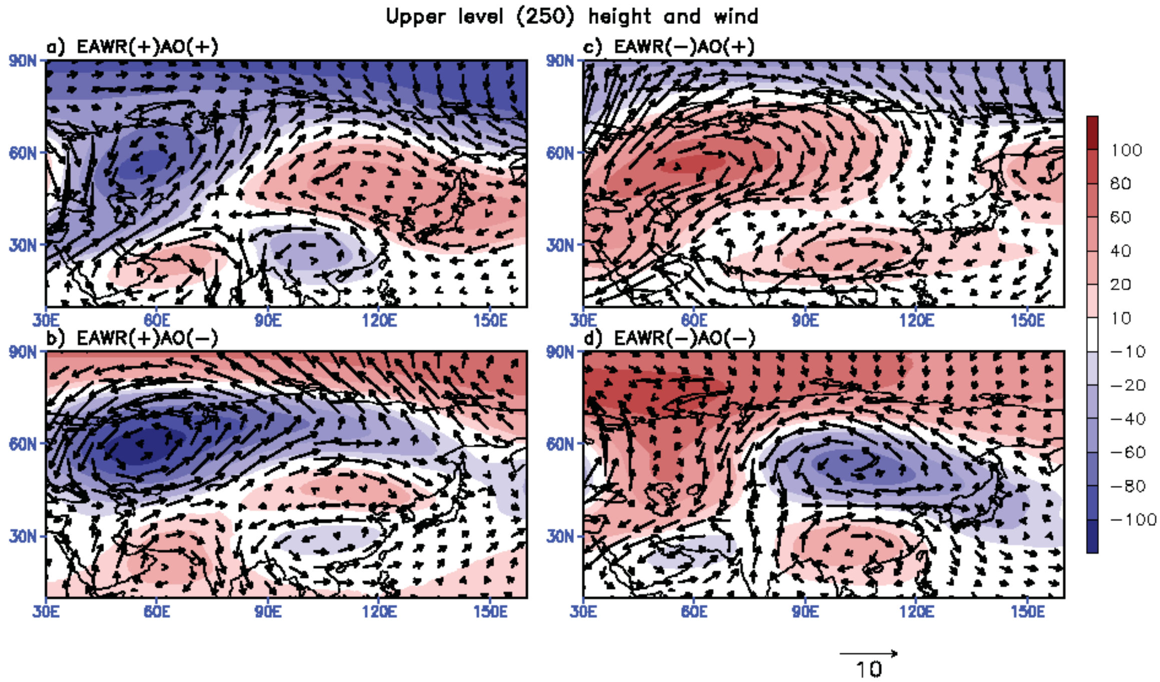

Figure 10. Composited distributions of the anomalous geopotential height (shaded) and wind at upper-level (250 hPa) for combined EA/WR and AO months. Each panel represents the combined effect of (a): EA/WR(+)AO(+), (b): EA/WR(+)AO(-), (c): EA/WR(-)AO(+), and (d): EA/WR(-)AO(-).

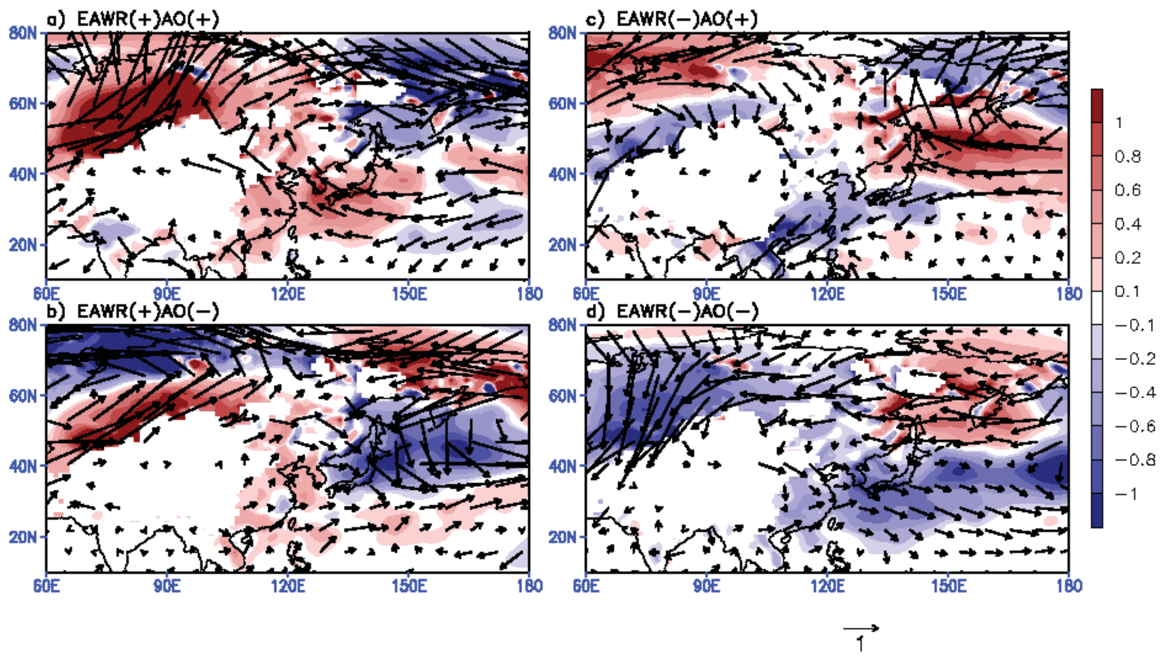

Figure 11. Same as Figure 10 but for advective temperature change [K/day] (shaded) by lower-level (850 hPa) winds.